Horizontal Density Structure and Restratification of the Arctic Ocean Surface Layer

MARY-LOUISE TIMMERMANS

Department of Geology and Geophysics, Yale University, New Haven, Connecticut

SYLVIA COLE AND JOHN TOOLE

Department of Physical Oceanography, Woods Hole Oceanographic Institution, Woods Hole, Massachusetts

ABSTRACT

Ice-tethered profiler (ITP) measurements from the Arctic Ocean's Canada Basin indicate an ocean surface layer beneath sea ice with significant horizontal density structure on scales of hundreds of kilometers to the order 1 km submesoscale. The observed horizontal gradients in density are dynamically important in that they are associated with restratification of the surface ocean when dense water flows under light water. Such restratification is prevalent in wintertime and competes with convective mixing upon buoyancy forcing (e.g., ice growth and brine rejection) and shear-driven mixing when the ice moves relative to the ocean. Frontal structure and estimates of the balanced Richardson number point to the likelihood of dynamical restratification by isopycnal tilt and submesoscale baroclinic instability. Based on the evidence here, it is likely that submesoscale processes play an important role in setting surface-layer properties and lateral density variability in the Arctic Ocean.

1. Introduction

Properties and dynamics of the Arctic Ocean are of major significance to the climatically important influence of the ocean on sea ice. The only direct ocean impact to ice cover is through the 10–40-m-thick surface ocean layer[1] overlying the Arctic halocline. The halocline is characterized by a strong increase in salinity with depth and temperatures close to the freezing point, although with warmer Pacific Ocean layers in the Canadian Basin (Steele and Boyd 1998; Boyd et al. 2002; Steele et al. 2004). The halocline separates warmer water of North Atlantic origin at 250–800-m depth from the surface layer and overlying sea ice. This analysis focuses on the surface layer beneath ice cover in the Arctic Ocean's Canada Basin; many properties of this layer,

such as its depth and temperature, influence ice growth and melt and are crucial to Arctic climate predictions.

The Arctic surface layer is most often examined within the framework of its vertical structure because the strong halocline stratification impedes vertical fluxes of deep-ocean heat to the surface and sea ice (e.g., Toole et al. 2010). In the one-dimensional view, the surface layer is mixed by convection (e.g., upon ice growth and brine rejection) and shear-driven mixing when the ice moves relative to the ocean, whereas surface-layer restratification takes place upon warming and surface freshening by ice melt and river runoff. However, studies in the midlatitude ice-free oceans have demonstrated that surface-layer properties are not set by vertical processes alone: the evolution of the surface layer can be additionally influenced by horizontal density gradients, or fronts, and ageostrophic flows that develop at fronts in the surface layer (e.g., Brainerd and Gregg 1993; Tandon and Garrett 1994; Haine and Marshall 1998; Boccaletti et al. 2007; Thomas et al. 2008). These submesoscale [$O(1)$ km horizontal scale] processes have been found to be active in the ocean's surface layer, which is characterized by weak stratification and a relatively small Rossby deformation radius [$O(1)$ km]. This study presents these ideas in the context of sea ice cover

---

[1] Note that to avoid confusion, we do not use the more common term "mixed layer" in reference to the surface layer because this layer can be weakly stratified.

Corresponding author address: Mary-Louise Timmermans, Department of Geology and Geophysics, Yale University, 210 Whitney Ave., New Haven, CT 06515.
E-mail: mary-louise.timmermans@yale.edu

and gives a preliminary analysis of the horizontal structure of the Arctic surface layer and its impact on restratification.

Horizontal density gradients occur in the surface layer because of spatially variable surface forcing (e.g., a local storm or ice growth and brine rejection in an open-water lead) or the cascade from large to small scales of existing gradients through horizontal stirring. Restratification of the upper ocean can then take place when vertical isopycnals (horizontal density gradients) slump under gravity and more dense fluid flows under adjacent lighter waters. Rotation limits the gravitational slumping leading to a state in which horizontal density gradients exist in geostrophic balance (Tandon and Garrett 1994). A restratified surface layer with tilted isopycnals and light water over dense water results. Surface fronts can become baroclinically unstable to instabilities with growth rates on the order of 1 day, which grow to form eddies in the surface layer that continue the restratification (Boccaletti et al. 2007; Fox-Kemper et al. 2008). Modeling studies indicate that such eddies can form sufficiently fast to restratify the upper ocean in between events that mix vertically (Boccaletti et al. 2007). Observations confirm that submesoscale restratification is actively occurring in the midlatitudes (Rudnick and Ferrari 1999; Ferrari and Rudnick 2000; Rudnick and Martin 2002; Hosegood et al. 2006, 2008; Cole et al. 2010). Submesoscale restratification has not been examined under sea ice.

Climate models will not be capable of resolving the submesoscales in the near future—the effects of motions at these scales need to be parameterized. One such parameterization for upper-ocean restratification by submesoscale, surface-layer eddies has been formulated to represent temperature, salinity, and tracer fluxes otherwise missing in coarse-resolution models (Fox-Kemper et al. 2008, 2011). Comparisons between coarse-resolution models implementing the parameterization of Fox-Kemper et al. (2008) and submesoscale eddy-resolving simulations suggest the parameterization is appropriate (Fox-Kemper and Ferrari 2008). Direct comparisons to data are limited because of the inherent difficulties in observing submesoscale processes in the ocean surface layer. Comparing models with and without the parameterization shows that the largest reduction in surface-layer depth from submesoscale restratification is in the polar regions, with an accompanying redistribution in sea ice thickness that appears to be connected to the reduced surface-layer heat capacity when the parameterization is used (Fox-Kemper et al. 2011). Such a parameterization may improve some pan-Arctic and global models that overestimate the magnitude of the winter surface-layer depth in some regions of the Arctic (Zhang

and Steele 2007; Golubeva and Platov 2007; Holloway et al. 2007; Popova et al. 2010).

In an observational study, guided by a numerical ocean mixed-layer model, Toole et al. (2010) analyzed Arctic Ocean surface-layer measurements from autonomous ocean profiling instruments, ice-tethered profilers (ITPs; Krishfield et al. 2008), sea ice observations from ice mass balance buoys, and atmosphere–ocean heat fluxes to conclude that the strong density stratification at the base of the surface layer greatly impedes the flux of deep-ocean heat to the layer in contact with sea ice. However, the one-dimensional model employed by Toole et al. (2010) could not reproduce the observed variability in surface-layer stratification, suggesting that restratification by submesoscale processes, not represented in the one-dimensional framework, may be occurring.

Since the start of the ITP program in 2004, ITP measurements have been returned from all Arctic basins (Toole et al. 2011) and constitute a rich dataset for the analysis of horizontal variability in the ocean surface layer. ITPs mounted in the permanent sea ice cover enable examination at high spatial and temporal resolution of upper-ocean processes without the influence of a ship (compared to standard hydrographic surveys). As the underpinning to a basinwide analysis of lateral surface-layer dynamics, in this paper we analyze ITP measurements from the Canada Basin in winter 2009/10, which include some of the highest spatial and temporal resolutions, to demonstrate the role of submesoscale lateral processes in regulating upper-ocean properties. In the next section, we describe the ITP systems and observations. In section 3, we define the surface layer and characterize vertical density gradients within this layer. In section 4, we examine the scales of horizontal variability in the surface layer, analyze examples of surface fronts, and assess whether restratification by ageostrophic baroclinic instability may contribute to restratification in the upper Arctic Ocean. Our results are summarized and discussed in section 5.

2. Ice-tethered profiler measurements

ITPs are automated profiling systems that repeatedly sample water properties beneath sea ice for periods of up to 3 yr. The ITP system consists of three components: a surface instrument package that sits atop an ice floe and houses an inductive modem, a GPS receiver, and an Iridium satellite phone; a wire-rope tether extending from the surface package through the ice to about 750-m depth; and an instrumented underwater profiling unit that travels up and down the wire tether from 1 to 5 m below the base of the ice to 750-m depth on a preprogrammed
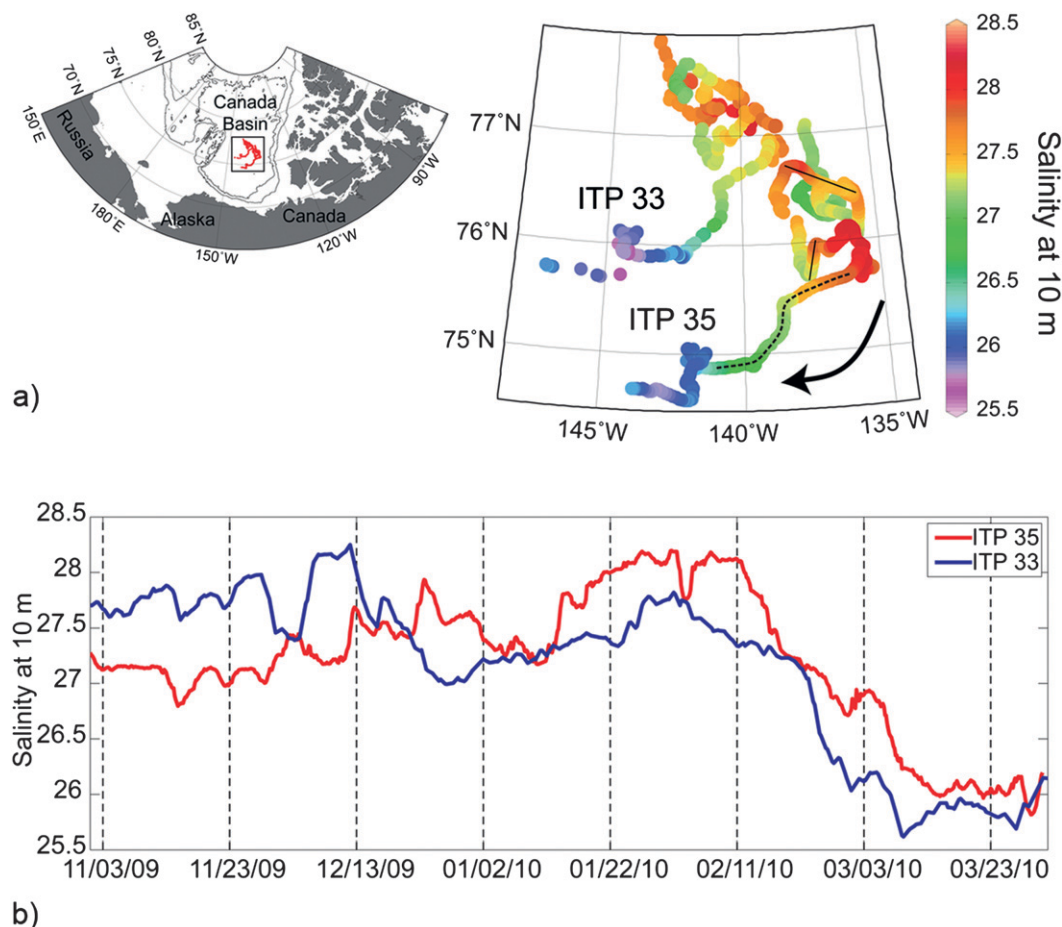
FIG. 1. (a) Maps showing drift tracks and profile locations of ITPs 33 and 35 and salinity at 10 m between 1 Nov 2009 and 1 Apr 2010 (a total of 1159 profiles through the surface layer); (left) The 1000- and 2500-m isobaths are plotted. (right) Drift was from north to southwest, as shown by the black arrow. The two straight lines on the ITP 35 drift track mark the sections plotted in Fig. 5, and the dotted line marks the relatively straight 200-km segment used in the spectral analysis (Fig. 4). (b) Time series of salinity at 10 m measured by ITPs 33 and 35 corresponding to the profile locations shown in (a).

sampling schedule. The profiling vehicle houses a conductivity–temperature–depth (CTD) sensor package that samples at 1 Hz and the vehicle profiles at a speed of about 25 cm s^{-1}, so that the raw data have a vertical resolution of around 25 cm. ITP sensor data are transmitted from the underwater profiler to the surface buoy via modem and relayed to shore via Iridium satellite [technical details of the ITP system and data processing procedures are given in Krishfield et al. (2008) and at http://www.whoi.edu/itp]. Data from the ITPs are processed immediately upon transmission and made directly available on the web (http://www.whoi.edu/itp/data). After calibration and processing ITP temperature, pressure, and salinity data accuracies are estimated to be ±0.001°C, ±1 dbar, and ±0.002, respectively.

In this study, we analyze measurements from two ITPs (ITP system numbers 33 and 35) that operated in 2009/10 in the Canada Basin (Fig. 1). The ITPs did not sample shallower than about 1–5 m below the underside of the ice, whereas regional surface mixed layers in the summer months (typically July and August) can be thinner than this (Toole et al. 2010). For this reason and to lessen the complicating effects of summer buoyancy fluxes and meltwater input, we restrict our analysis to the winter season (1 November 2009 to 1 April 2010). ITP 33 returned 2 profiles per day and ITP 35 returned 6 profiles per day, with typical ice-drift speeds of around 5–15 cm s^{-1}. Profile spacing was 3.7 ± 3.2 km for ITP 33 and 1.4 ± 0.9 km for ITP 35.

3. Defining the surface layer

To characterize the surface layer, we need a criterion that accurately specifies its thickness. Here, we define the surface-layer base by a critical density difference,
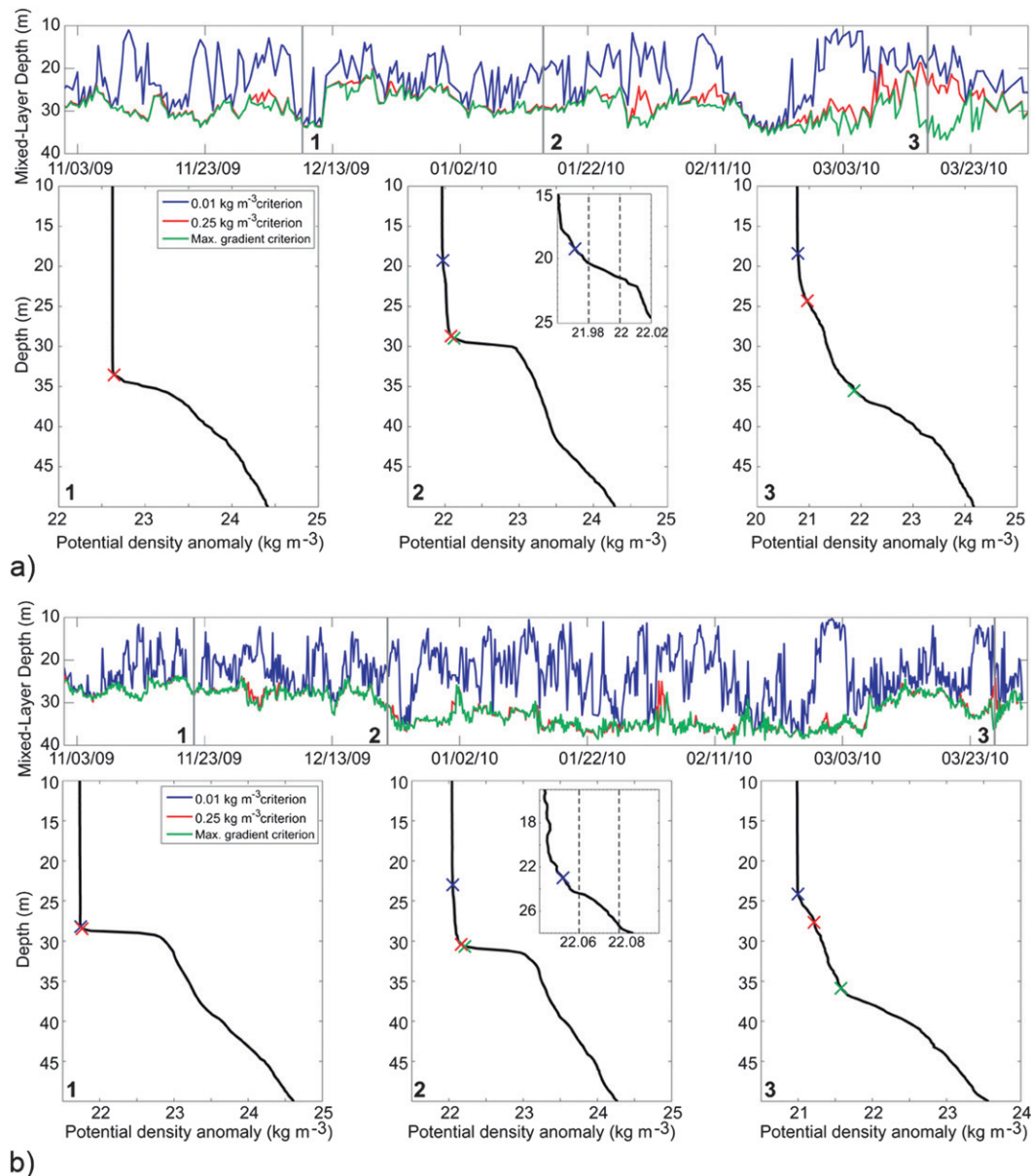
FIG. 2. Time series of surface-layer depth are shown at the top for (a) ITP 33 with 2 observations per day and (b) ITP 35 with 6 observations per day. Surface-layer depth is computed by two different methods, using a critical density difference criterion of 0.25 kg m^{-3} and a gradient method as described in the text. A mixing layer depth is computed using a critical density difference criterion of 0.01 kg m^{-3}. Representative potential density anomaly profiles are shown below for cases 1) where all three methods agree, 2) where a mixing layer is present and the 0.01 kg m^{-3} criterion differs from the 0.25 kg m^{-3} and maximum gradient criteria, and 3) where the two surface-layer depths differ and the base of the surface layer is less well defined.

taken to be 0.25 kg m^{-3}, from the shallowest measurement. Given the strong stratification at its base on the order of 0.5 kg m^{-4}, surface-layer depth is insensitive to the exact critical density difference chosen (e.g., see profiles in Fig. 2). Moreover, the result of this method does not deviate significantly from a gradient method where the surface-layer depth is taken to be the point

where the vertical density gradient is maximum between the surface and 70-m depth (Fig. 2). [Various methods for specifying mixed-layer depth are reviewed in Holte and Talley (2009).]

Toole et al. (2010) define the Arctic mixed layer as the depth range in which potential density (referenced to 0 dbar) remains within 0.01 kg m^{-3} of the shallowest

value (ITP density accuracy is about ± 0.002 kg m^{-3}) on the assumption that density overturning may be suppressed below depths where the density exceeds the shallowest value by more than 0.01 kg m^{-3} (see, e.g., Brainerd and Gregg 1993). With this criterion, the term mixed layer is more appropriate. Toole et al. (2010) found that observed winter mixed layer depths in the Canada Basin varied from about 10 m to about 30–40 m over a few days, whereas their one-dimensional model showed sustained mixed layer thicknesses at the deep end of the observed range over the course of the simulations. We will show here that this discrepancy between model and observations is likely due to submesoscale restratification. In this study, we make the distinction between homogeneous mixing layers captured by the stricter criterion of Toole et al. (2010) and the surface layer marked by the clear barrier of the strong halocline that impedes vertical heat fluxes from the deep ocean through the base of the surface layer. Although microstructure measurements are the most accurate way to quantify active mixing layers (Brainerd and Gregg 1993), gradients at the base of the observed Arctic mixing layers are sufficiently small that molecular diffusion would erase them in a few days. Mixing layers defined using the 0.01 kg m^{-3} criterion represent layers that are actively mixing or have been very recently mixed. When a mixing layer is present, the underlying portion of the surface layer can act as a barrier layer that prevents deep-ocean heat from being entrained to the surface; this is discussed further in section 5.

Mixing layers (apparent where the 0.01 kg m^{-3} criterion differs from the 0.25 kg m^{-3} criterion) are a common occurrence throughout ITP 33 and 35 winter time series (Fig. 2) and are present in about 50% of the profiles. These are likely a manifestation of lateral mixed layer restratification when, at least in winter, the generation of a relatively fresh mixing layer in the top of the surface layer cannot be attributed to melt. In the presence of a mixing layer, a relatively weak density gradient is observed at its base, whereas when the surface layer is vertically homogenized a stronger gradient is seen. Histograms of the density gradient across the mixing layer base (defined by the 0.01 kg m^{-3} criterion) have a bimodal structure (Toole et al. 2010). It follows that there is a correlation between the density gradient at the base of a mixing layer and its depth.

4. Horizontal density structure of the surface layer

Horizontal temperature–salinity structure under sea ice differs from that in ice-free oceans. In the midlatitude ice-free oceans, the indirect signature of submesoscale restratification is pervasive density compensation (i.e.,
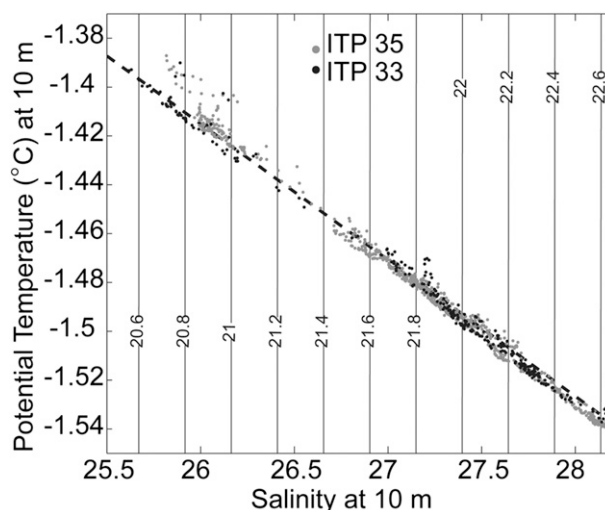

FIG. 3. Potential temperature vs salinity at 10 m (from 1159 profiles through the surface layer as shown in Fig. 1). Isopycnals (potential density anomaly referenced to the surface) are shown by the nearly vertical gray lines. Most points lie near the dashed freezing line (for pressure = 1 dbar) with some exceptions; departures from freezing are associated with anomalously warm water below the base of the surface layer as encountered by the ITPs between around 25 Mar and 1 Apr ($S \sim 26$).

horizontal temperature and salinity gradients in the mixed layer that cancel in their effect on density) at small lateral scales (Rudnick and Ferrari 1999; Ferrari and Rudnick 2000; Rudnick and Martin 2002; Hosegood et al. 2006, 2008; Cole et al. 2010). Restratification by frontal slumping and surface-layer instabilities that bring dense water beneath light water, followed by vertical mixing, efficiently destroys lateral density gradients, leaving behind only compensated temperature–salinity gradients. Beneath sea ice, however, the Arctic Ocean winter surface layer is almost always at the surface freezing temperature for seawater (Fig. 3), and we do not observe density compensation. Additionally, destruction of lateral density gradients in the midlatitudes is most effective when vertical mixing is strongest, such as in winter: gradients tilt, mix vertically, and then tilt and mix again in rapid succession (Rudnick and Martin 2002; Cole et al. 2010). Weaker vertical mixing under sea ice may affect horizontal density structure in the Arctic.

Horizontal density gradients are prevalent at all observed scales. The ITPs analyzed here drifted about 250 (ITP 33) and 320 km (ITP 35) from their starting locations over the course of winter 2009/10, with cumulative along-track distances for their circuitous drifts of about 1200 km for each track. Both ITPs sampled a clear large-scale gradient from high to low upper-ocean salinity (Fig. 1) as the ITPs drifted southwest toward the center

of the Beaufort Gyre (a major atmosphere–ice–ocean anticyclonic circulation system centered in the Canada Basin; see, e.g., Proshutinsky et al. 2009). Superimposed on this larger-scale spatial gradient are mesoscale and submesoscale fluctuations. Temporal variability was evident during the early part of the drift, with profiles overlying in space having different salinity. Such temporal variability was relatively small compared with observed spatial changes.

Wavenumber spectral analysis is used to describe the horizontal potential density variance in the surface layer over wavelengths of 2–100 km. This is reasonable because ITP drift speeds were around 10 km day^{-1}, which is faster than the evolution of both submesoscale features [$O(1)$ km and $O(1)$ day] and mesoscale features [$O(10)$ km and $O(10)$ days]. Furthermore, even though the drift tracks are not straight segments, features at these scales should have no preferred x–y orientation. Note that, deeper than the upper few meters and depending on under-ice morphology, the ocean velocity is typically much smaller than the ice velocity. Further, ice and ocean flows do not align; boundary layer currents under drifting ice exhibit Ekman spirals and the Ekman transport is about 40° to the right of the direction of the ice–ocean stress (McPhee 2008, and references therein).

Only observations from ITP 35 are considered because of its more rapid profiling schedule and corresponding higher horizontal resolution. Spectra were computed by interpolating 200-km potential density segments (referring to cumulative distance along the ITP drift track) onto a 1-km uniform grid, removing a trend, averaging the resulting Fourier coefficients in wavenumber bands with more degrees of freedom at higher wavenumbers, and truncating at a 2-km wavelength. Wavenumber spectra were calculated for six consecutive 200-km segments sampled by ITP 35, which were then averaged, as well as for one relatively straight 200-km section sampled between 11 February and 7 March 2010 (Fig. 4). The best-fit slopes for 10-m potential density variance (Fig. 4a) over 5–50 km wavelengths are -2.9 ± 0.2 for the full record and -2.7 ± 0.6 for the single straight section. Spectral slopes are indistinguishable from k^{-3} (k: horizontal wavenumber). Wavenumber spectra at other depths within the surface layer are essentially identical.[2] This differs from the midlatitudes where spectra of horizontal surface-layer
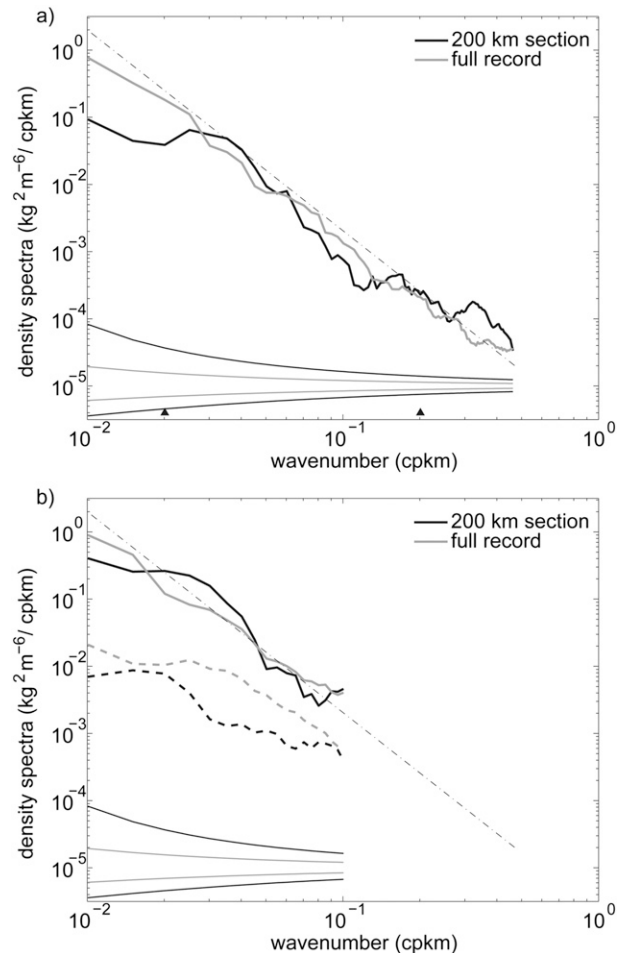

FIG. 4. Horizontal wavenumber spectra of potential density variance from a relatively straight 200-km segment (referring to a cumulative along-track distance and indicated by the dotted line in Fig. 1) and from six consecutive 200-km segments, which were then averaged (full record), of ITP 35 drift in winter 2009/10: (a) at 10-m depth in the surface layer and (b) at 60- (solid) and 110-m (dashed) depths below the surface layer. The dashed–dotted line has a slope of k^{-3}. Triangles in (a) correspond to 5 and 50 km wavelengths. The 95% confidence intervals are shown. The number of degrees of freedom at each wavelength is taken to be twice the record length, 200 km, divided by the wavelength. The six 200-km segments are assumed to be independent. Spectra below the surface layer are not considered at wavelengths smaller than 10 km because internal waves alias vertical gradients into horizontal structure at these scales.

density or temperature have been found to scale as k^{-2} for scales between $O(1)$ and $O(100)$ km (e.g., Samelson and Paulson 1988; Hodges and Rudnick 2006; Cole et al. 2010). Note the relatively steep horizontal wavenumber spectra found here suggest less energetic small-scale structure than the k^{-2} scaling and are more consistent with k^{-3} quasigeostrophic turbulence scaling (Charney 1971). Knowledge only of the spectral slope is of course not sufficient to determine the physical mechanisms at

---

[2] Spectral slopes deeper than the surface layer (Fig. 4b) over 10–50-km wavelengths are indistinguishable from k^{-3}; spectra below the surface layer are not considered at wavelengths smaller than 10 km because internal waves alias vertical gradients into horizontal structure at these scales.
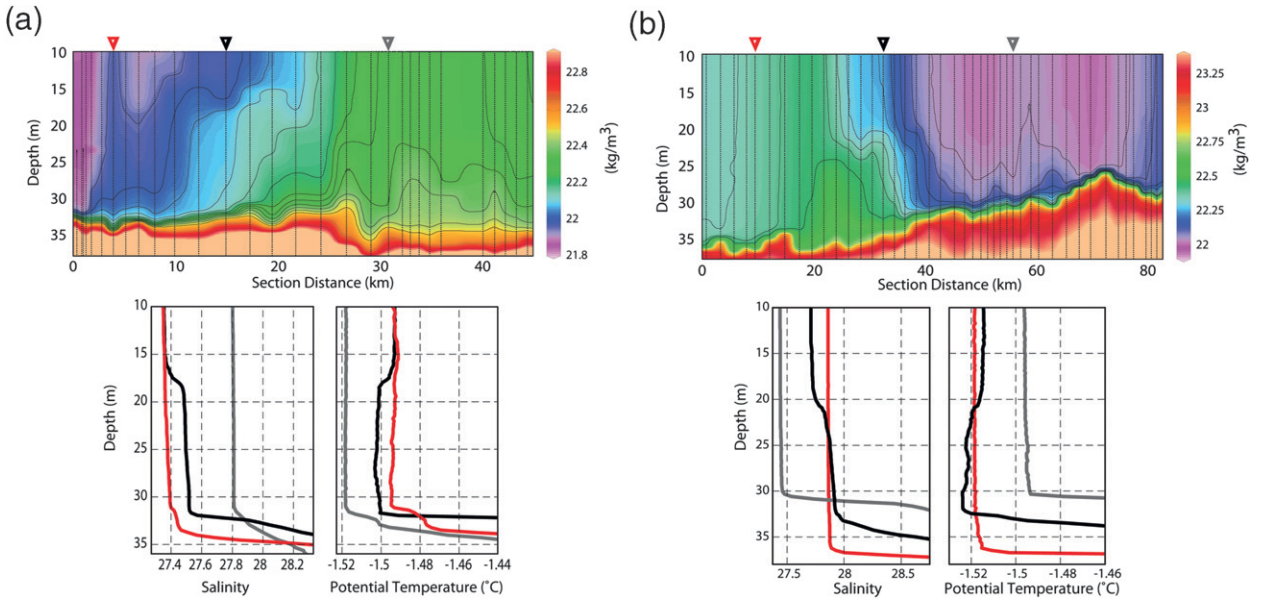
FIG. 5. (top) Representative surface fronts sampled by ITP 35 from straight portions of ITP drift tracks. Depth–distance sections are of potential density (kg m^{-3}) anomaly (referenced to 0 dbar) with contours spaced by 0.05 kg m^{-3}. Thin vertical lines mark profile locations. (bottom) Profiles of salinity and potential temperature at the positions marked on the sections by the inverted triangles, which are centered on the front (black) and to either side of the front (red and gray). (a) South–north section in January 2010 in the Canada Basin near 76°N, 138°W, along the southernmost straight line drawn on the ITP 35 drift track in Fig. 1. (b) West–east section in December 2009 in the Canada Basin near 76.5°N, 137°W, along the northernmost straight line drawn on the ITP 35 drift track in Fig. 1.

play. We speculate that the dynamical processes of frontogenesis and instability may be altered by the presence of sea ice and ice–ocean shear; further analysis is needed to examine how differing physical processes in the surface Arctic Ocean under ice cover might produce a steeper spectral slope than found in the midlatitude ice-free oceans.

Two representative segments depicting fronts encountered by ITP 35 give evidence for restratification by frontal slumping. Both fronts were 20–30-km-wide regions of tightly spaced isopycnals that were tilted in the horizontal (around an along-section distance of 15–25 km in Fig. 5a and 25–40 km in Fig. 5b). These surface fronts have horizontal density gradients of about 0.04 kg m^{-3} km^{-1}, although this is an underestimate if the section is not perpendicular to the front. Profiles at the fronts and on either side (Fig. 5, bottom) suggest surface-layer restratification with mixing layers associated with lateral isopycnal slumping (rather than a one-dimensional process). Note that the entire surface layer is at the freezing temperature with the relatively fresh mixing layers warmer than the relatively salty water in the deeper part of the surface layer. These examples in combination with the numerous mixing layers apparent in the surface-layer depth time series (Fig. 2) provide evidence for the pervasiveness of lateral restratification (recall that ice melt and warming do not typically occur

in winter, so a mixing layer will not develop from one-dimensional processes).

It is useful to introduce the balanced Richardson number defined as Ri $\equiv f^2N^2/M^4$, where $N^2 \equiv -(g/\rho_0)(\Delta\rho/H)$ is the vertical buoyancy gradient within the surface-layer of depth H and $M^2 \equiv -(g/\rho_0)\partial\rho/\partial x$ $(=\partial b/\partial x)$ is the horizontal buoyancy gradient in the vicinity of the front ($\Delta\rho$ is the density difference between the top and the base of the surface layer, ρ_0 is a reference density, and $f \approx 1.41 \times 10^{-4}$ s^{-1} is the Coriolis frequency). Tandon and Garrett (1994) showed that, for a given initial buoyancy $b(x)$, where x is the direction of the maximum buoyancy gradient, the maximum Richardson number (as defined above) that can be attained by geostrophic adjustment is given by Ri$_{max}$ = $(1 - |b_{xx}|H/2f^2)^{-1}$. For Richardson numbers $\gtrsim 1$, surface fronts may be unstable to ageostrophic baroclinic instabilities (e.g., Stone 1966; Molemaker et al. 2005; Boccaletti et al. 2007), which contribute to surface-layer restratification by drawing upon the potential energy of horizontal density gradients; restratification by submesoscale eddies increases the balanced Richardson number (cf. Fox-Kemper et al. 2008).

Richardson numbers can be estimated for the representative fronts and the observed submesoscale density gradients. For the representative fronts (Fig. 5), $M^2 \approx 4 \times 10^{-7}$ s^{-2}, $N \approx 0.005$ s^{-1}, and $H \approx 32$ m, which yields

$Ri \approx 3$. Richardson numbers of a similar magnitude may be fairly common in the surface layer. Considering all adjacent profiles with horizontal spacing less than 2 km (75% of ITP 35 profiles and 37% of ITP 33 profiles), we find the mean density gradient is about 0.03 ± 0.03 k gm^{-3} km^{-1}. Mean values of vertical buoyancy gradient and surface-layer depth over all ITP profiles (Fig. 1) are $N \approx 0.006$ s^{-1} and $H \approx 30$ m (these values are approximately the same if the mean is limited to only those surface-layer profiles exhibiting mixing layers), which yields $Ri \approx 8$.

A nondimensional frontal "narrowness" parameter $|b_{xx}|H/f^2$ can be estimated to assess the maximum Richardson number that can be reached by geostrophic adjustment. Examination of the representative fronts (Fig. 5) suggests that the horizontal buoyancy gradient reduces to about $\frac{1}{3}$ of its value over about 6 km (assuming ITP drift is normal to the front), which yields $|b_{xx}|H/f^2 \approx 0.04$. Therefore, for these fronts we expect $Ri_{max} \approx 1$ from geostrophic adjustment alone. It should be noted that stronger, narrower fronts are conceivable ($|b_{xx}|H/f^2 \rightarrow 1$) and would lead to larger maximal Richardson numbers in the geostrophically adjusted state. However, it is most likely that the formation of such sharp fronts would be prevented by shear and ageostrophic baroclinic instabilities. The estimated $Ri \gtrsim 1$ are consistent with the complicated structure in the vicinity of the representative fronts (Fig. 5), which may be associated with restratification by submesoscale eddies.

5. Discussion and summary

We observe surface-layer stratification that appears to be attributable to lateral processes. Analysis of surface-layer ITP measurements in the Canada Basin plus inferences from the results of past numerical and theoretical analyses suggests that submesoscale processes are actively driving surface-layer restratification in the Arctic. The steeper spectral slope (k^{-3} scaling) of horizontal potential density variance found in the surface Arctic Ocean under sea ice compared to in the midlatitude ice-free oceans (which exhibit a k^{-2} scaling) may suggest the influence of different physical mechanisms controlling horizontal structure between the two cases. Observations indicate balanced Richardson numbers $O(1)$ in the vicinity of fronts, suggesting that submesoscale eddies likely develop by ageostrophic baroclinic instability and restratify the surface layer.

The prevalence of nonnegligible stratification in the wintertime surface layer indicates that dynamical restratification may be sufficiently active to oppose convective and mechanical processes (ice growth and ice–ocean shear) that keep the layer vertically well mixed. It is

common to observe surface layers that consist of a shallow mixing layer (to which active turbulent mixing is confined) overlying a slightly denser, weakly stratified barrier layer. After this restratification, the portion of the surface layer below the shallow mixing layer can act as an insulating layer; active entrainment is at the base of the mixing layer, preventing ocean heat below the surface layer from being entrained to the surface. To examine the strength of this barrier, it is instructive to compare the potential energy increase associated with vertically mixing profiles with and without mixing layers to achieve a surface-layer temperature departure from freezing by the same amount. To do this, we homogenized each vertical potential temperature/salinity profile in 1-m increments until the resulting homogeneous surface-layer temperature was $0.05°C$ above the freezing temperature. For this end state, the potential energy increase is about 10% more for profiles with mixing layers. Because the surface layer is stratified in about 50% of the profiles, this amounts to an input of around 5% more turbulent kinetic energy required to achieve this particular final state. Although it may be that the impact of lateral restratification processes on the penetration depth of mixing events is relatively minor, modification to surface-layer properties by submesoscale restratification no doubt affects the heat budget of the surface Arctic Ocean (e.g., mixing layers result in solar insolation being distributed over a thinner region) and biological productivity (e.g., the mixing layer depth determines light levels available to phytoplankton for growth).

Key questions for future studies relate to how lateral restratification affects vertical heat fluxes in different regions of the Arctic (i.e., at the boundaries of the Beaufort gyre and in other regions of intensified horizontal density gradients) and how the frontal structure and associated geostrophic velocity shear and lateral exchanges will be modified by a seasonally and interannually evolving ice pack. Although we have only analyzed winter observations, submesoscale restratification is likely to affect surface-layer properties year-round. The present generation of ITPs provides a valuable exploratory assessment but can only marginally (or intermittently) resolve submesoscale length and time scales. Experiments with multiple buoys on one ice floe and more rapid sampling are planned to address these issues.

Coupled models of the Arctic are presently not resolving the small spatial scales of surface-layer instabilities that can modify heat, salt and momentum fluxes between the upper ocean and adjacent sea ice cover. The incorporation of a parameterization similar to that of Fox-Kemper et al. (2008) into regional Arctic Ocean models may lead to more accurate predictions of surface-layer evolution and ocean–ice–atmosphere interactions.

Note that the implementation of the Fox-Kemper et al. (2008) submesoscale restratification parameterization into coarse-resolution models relies on a k^{-2} relationship for which a scaling factor can be used to relate the strength of submesoscale fronts to fronts on the model grid scale (Fox-Kemper et al. 2011); in coarse-resolution models, modification would be needed to implement the parameterization when surface-layer density variance spectra do not satisfy a k^{-2} scaling law, as appears to be the case in the Arctic under sea ice. As well, numerical simulations that resolve submesoscale motions are needed to guide interpretation of observations of surface-layer restratification under sea ice.

REFERENCES

Boccaletti, G., R. Ferrari, and B. Fox-Kemper, 2007: Mixed layer instabilities and restratification. *J. Phys. Oceanogr.,* **37,** 2228–2250.

Boyd, T. J., M. Steele, R. D. Muench, and J. T. Gunn, 2002: Partial recovery of the Arctic Ocean halocline. *Geophys. Res. Lett.,* **29,** 1657, doi:10.1029/2001GL014047.

Brainerd, K., and M. Gregg, 1993: Diurnal restratification and turbulence in the oceanic surface mixed layer—Part 1: Observations. *J. Geophys. Res.,* **98,** 22 645–22 656.

Charney, J., 1971: Geostrophic turbulence. *J. Atmos. Sci.,* **28,** 1087–1095.

Cole, S. T., D. L. Rudnick, and J. A. Colosi, 2010: Seasonal evolution of upper-ocean horizontal structure and the remnant mixed layer. *J. Geophys. Res.,* **115,** C04012, doi:10.1029/2009JC005654.

Ferrari, R., and D. L. Rudnick, 2000: Thermohaline variability in the upper ocean. *J. Geophys. Res.,* **105** (C7), 16 857–16 883.

Fox-Kemper, B., and R. Ferrari, 2008: Parameterization of mixed layer eddies. Part II: Prognosis and impact. *J. Phys. Oceanogr.,* **38,** 1166–1179.

——, ——, and R. Hallberg, 2008: Parameterization of mixed layer eddies. Part I: Theory and diagnosis. *J. Phys. Oceanogr.,* **38,** 1145–1165.

——, and Coauthors, 2011: Parameterization of mixed layer eddies. III: Implementation and impact in global ocean climate simulations. *Ocean Modell.,* **39** (1–2), 61–78, doi:10.1016/j.ocemod.2010.09.002.

Golubeva, E. N., and G. A. Platov, 2007: On improving the simulation of Atlantic Water circulation in the Arctic Ocean. *J. Geophys. Res.,* **112,** C04S05, doi:10.1029/2006JC003734.

Haine, T., and J. Marshall, 1998: Gravitational, symmetric, and baroclinic instability of the ocean mixed layer. *J. Phys. Oceanogr.,* **28,** 634–658.

Hodges, B. A., and D. L. Rudnick, 2006: Horizontal variability in chlorophyll fluorescence and potential temperature. *Deep-Sea Res. I,* **53,** 1460–1482.

Holloway, G., and Coauthors, 2007: Water properties and circulation in Arctic Ocean models. *J. Geophys. Res.,* **112,** C04S03, doi:10.1029/2006JC003642.

Holte, J., and L. Talley, 2009: A new algorithm for finding mixed layer depths with applications to Argo data and Subantarctic Mode Water formation. *J. Atmos. Oceanic Technol.,* **26,** 1920–1939.

Hosegood, P., M. C. Gregg, and M. H. Alford, 2006: Sub-mesoscale lateral density structure in the oceanic surface mixed layer. *Geophys. Res. Lett.,* **33,** L22604, doi:10.1029/2006GL026797.

——, ——, and ——, 2008: Restratification of the surface mixed layer with submesoscale lateral density gradients: Diagnosing the importance of the horizontal dimension. *J. Phys. Oceanogr.,* **38,** 2438–2460.

Krishfield, R., J. Toole, A. Proshutinsky, and M.-L. Timmermans, 2008: Automated ice-tethered profilers for seawater observations under pack ice in all seasons. *J. Atmos. Oceanic Technol.,* **25,** 2091–2095.

McPhee, M., 2008: *Air-Ice-Ocean Interaction: Turbulent Ocean Boundary Layer Exchange Processes.* Springer, 215 pp.

Molemaker, M. J., J. C. McWilliams, and I. Yavneh, 2005: Baroclinic instability and loss of balance. *J. Phys. Oceanogr.,* **35,** 1505–1517.

Popova, E. E., A. Yool, A. C. Coward, Y. K. Aksenov, S. G. Alderson, B. A. de Cuevas, and T. R. Anderson, 2010: Control of primary production in the Arctic by nutrients and light: Insights from a high resolution ocean general circulation model. *Biogeosciences,* **7,** 3569–3591, doi:10.5194/bg-7-3569-2010.

Proshutinsky, A., and Coauthors, 2009: Beaufort Gyre freshwater reservoir: State and variability from observations. *J. Geophys. Res.,* **114,** C00A10, doi:10.1029/2008JC005104.

Rudnick, D. L., and R. Ferrari, 1999: Compensation of horizontal temperature and salinity gradients in the ocean mixed layer. *Science,* **283,** 526–529, doi:10.1126/science.283.5401.526.

——, and J. P. Martin, 2002: On the horizontal density ratio in the upper ocean. *Dyn. Atmos. Oceans,* **36,** 3–21.

Samelson, R. M., and C. Paulson, 1988: Towed thermistor chain observations of fronts in the subtropical North Pacific. *J. Geophys. Res.,* **93,** 2237–2246.

Steele, M., and T. Boyd, 1998: Retreat of the cold halocline layer in the Arctic Ocean. *J. Geophys. Res.,* **103,** 10 419–10 435.

——, J. Morison, W. Ermold, I. Rigor, M. Ortmeyer, and K. Shimada, 2004: Circulation of summer Pacific halocline water in the

Arctic Ocean. *J. Geophys. Res.,* **109,** C02027, doi:10.1029/2003JC002009.

Stone, P., 1966: On non-geostrophic baroclinic stability. *J. Atmos. Sci.,* **23,** 390–400.

Tandon, A., and C. Garrett, 1994: Mixed layer restratification due to a horizontal density gradient. *J. Phys. Oceanogr.,* **24,** 1419–1424.

Thomas, L., A. Tandon, and A. Mahadevan, 2008: Sub-mesoscale processes and dynamics. *Ocean Modeling in an Eddying Regime, Geophys. Monogr.,* Vol. 177, Amer. Geophys. Union, 17–38.

Toole, J. M., M.-L. Timmermans, D. K. Perovich, R. A. Krishfield, A. Proshutinsky, and J. A. Richter-Menge, 2010: Influences of the ocean surface mixed layer and thermohaline stratification on Arctic sea ice in the central Canada Basin. *J. Geophys. Res.,* **115,** C10018, doi:10.1029/2009JC005660.

——, R. A. Krishfield, M.-L. Timmermans, and A. Proshutinsky, 2011: The ice-tethered profiler: Argo of the Arctic. *Oceanography,* **24,** 126–135.

Zhang, J., and M. Steele, 2007: Effect of vertical mixing on the Atlantic Water layer circulation in the Arctic Ocean. *J. Geophys. Res.,* **112,** C04S04, doi:10.1029/2006JC003732.